

Tensor Network States with Three-Site Correlators

Arseny Kovyrshin and Markus Reiher¹

ETH Zürich, Laboratorium für Physikalische Chemie, Vladimir-Prelog-Weg 2,
8093 Zürich, Switzerland

Abstract

We present a detailed analysis of various tensor network parameterizations within the Complete Graph Tensor Network States (CGTNS) approach. We extend our 2-site CGTNS scheme by introducing 3-site correlators. For this we devise three different strategies. The first relies solely on 3-site correlators and the second on 3-site correlators added on top of the 2-site correlator ansatz. To avoid an inflation of the variational space introduced by higher-order correlators, we limit the number of higher-order correlators to the most significant ones in the third strategy. Approaches for the selection of these most significant correlators are discussed. The sextet and doublet spin states of the spin-crossover complex manganocene serve as a numerical test case. In general, the CGTNS scheme achieves a remarkable accuracy for a significantly reduced size of the variational space. The advantages, drawbacks, and limitations of all CGTNS parameterizations investigated are rigorously discussed.

Date: May 22, 2016

¹Corresponding author: markus.reiher@phys.chem.ethz.ch

1 Introduction

Electronic structure theory aims at providing accurate properties of molecules in their electronic ground and excited states. However, systematically improvable wave function methods are often computationally expensive and can even become unfeasible. This dilemma is particularly pressing for systems with strong static electron correlation, i.e., for those with dense one-electron states around the Fermi energy level showing a small gap.

For such cases, the Density-Matrix Renormalization Group (DMRG) method^{1,2,3} has evolved as a powerful alternative to exact diagonalization techniques such as Complete Active Space Self-Consistent Field (CAS-SCF) approaches.^{4,5,6,7,8,9,10,11,12,13,14,15} The success of DMRG is due to a polynomial scaling of the computational cost with respect to an increasing number of active orbitals, in contrast to the exponential scaling¹⁶ of CAS-based approaches. It was shown by Östlund and Rommer¹⁷ that the DMRG optimizes Matrix Product States (MPS) — one-dimensional chains of tensors that are a consequence of the algorithm which imposes a one-dimensional ordering of the molecular orbitals in the construction process of the total basis states.

In contrast to one-dimensional spin chains in solid-state physics, molecular systems governed by the full Coulomb interaction in general feature multidimensional entanglement for which the linear MPS ansatz is not well suited. This in turn may lead to convergence problems. Still, the DMRG optimization of MPSs can be beneficial for strongly correlated molecules if other approaches are unfeasible as we pointed out for transition metal complexes.¹⁸ Moreover, dynamic correlation effects have to be considered — either a posteriori by perturbation theory^{19,20,15,21} or from the outset by, for example, short-range DFT.^{22,23}

One can overcome the problem of complex, multidimensional entanglement patterns by generalizing the MPS ansatz (see Ref. 14 for a discussion in the context of electronic structure theory). In the field of solid-state physics, the Tensor Product Variational Approach (TPVA),^{24,25,26,27} String Bond States (SBS),²⁸ Projected Entangled Pair States (PEPS),²⁹ Multiscale Entanglement Renormalization Ansatz (MERA),³⁰ Entangled Plaquette States³¹ (EPS), and Correlator Product States (CPS)³² attempt to generalize the MPS ansatz and describe multidimensional entanglement. These approaches constitute a new family of states called Tensor Network States (TNS).

Complete-Graph Tensor Network States (CGTNS)³³ were the first TNS application in quantum chemistry employing the full electronic Hamiltonian. The complexity of the

high-dimensional coefficient tensor was reduced by breaking it down into a complete-graph tensor network, in which all spin orbitals are connected with each other by 2-site correlators. The number of variational parameters is explicitly defined by the number of spin orbital pairs, which limits the variational freedom of the CGTNS ansatz for large active spaces.

Another TNS approach explored in the field of quantum chemistry are Tree Tensor Network States (TTNSs).^{34,35} While representing an interesting class of quantum states, the optimization of TTNS parameters can be cumbersome and non-competitive when compared to efficient traditional quantum chemical methods. In 2013, Nakatani and Chan proposed a TTNS variant for the full electronic Hamiltonian³⁶ that overcomes this problem. Tensors are connected as defined by a tree graph in TTNS, which attempt to map the molecular structure. Due to the absence of loops in their TTNS ansatz, Nakatani and Chan could apply the DMRG optimization algorithm.

The MPS ansatz is computationally very efficient, but truly reliable only for encoding a sequential entanglement structure. The TTNS scheme provides a more general description of entanglement which is, in the Nakatani–Chan formulation, of similar computational efficiency as MPS-DMRG, but it still imposes restrictions on the entanglement structure. CGTNS, in principle, does not restrict the entanglement pattern and works as well for multidimensional entanglement as it does for one-dimensional entanglement. However, the optimization of 2-site correlators is difficult as an efficient global and local optimization strategy is required. It is desirable to have an ansatz which adjusts the number of variational parameters to the system under study. Therefore, here we propose the concept of a CGTNS ansatz that starts from 2-site correlators and gradually include higher-order correlators. We then explore different optimization strategies to assess its potential for actual applications in molecular physics and chemistry.

2 Theory

2.1 Exact Solution

The eigenstate $|\Psi\rangle$ of electronic Hamiltonian H for an N -electron molecular system in non-relativistic quantum mechanics can be expressed as a linear combination of all Slater determinants contained in the $\binom{M}{N}$ -dimensional subspace $F(M, N)$ of the

2^M -dimensional Fock space $F(M)$,

$$|\Psi\rangle = \sum_{n_1 n_2 \dots n_M} C_{n_1 n_2 \dots n_M} |n_1 n_2 \dots n_M\rangle, \quad (1)$$

where M is the total number of spin orbitals constructed within a given one-electron basis set, and $|n_1 n_2 \dots n_M\rangle$ is an occupation number vector (ONV) representing a Slater determinant in the second quantization formalism. It is constructed as a tensor product of spin orbitals (sites) $|n_i\rangle$,

$$|n_1 n_2 \dots n_M\rangle \equiv |n_1\rangle \otimes |n_2\rangle \otimes \dots \otimes |n_M\rangle. \quad (2)$$

Every spin orbital can be “unoccupied” or “occupied”, $n_i = \{0, 1\}$, which yields a dimension of the local Hilbert space of two. Eq. (1) is called a Full Configuration Interaction (FCI) expansion. The coefficients $C_{n_1 n_2 \dots n_M}$ in Eq. (1) are obtained according to the variational principle which leads to the eigenvalue problem

$$\mathbf{H}\mathbf{C} = E\mathbf{C}, \quad (3)$$

where \mathbf{H} is the matrix representation of H in the determinant basis and \mathbf{C} is a vector of $C_{n_1 n_2 \dots n_M}$ coefficients for an electronic state of energy E . Since the number of Slater determinants that can be generated by distributing N electrons among M spin orbitals scales exponentially,¹⁶ the $C_{n_1 n_2 \dots n_M}$ can be found only for systems of limited size of up to about 18 electrons in 18 spatial orbitals. Hence, approximations are desirable for approaching the FCI solution in a given orbital space with more orbitals and electrons.

2.2 Tensor Network Decomposition

Tensor network approximations were suggested to reduce the dimensionality of a strongly correlated system. The TNS parameterizations mentioned in the introduction were investigated for model Hamiltonians such as the Heisenberg, Hubbard, Potts, and Ising Hamiltonians. The idea behind parameterizations such as TPVA, SBS, EPS, and CPS is similar, which can be seen in the work by Changlani *et al.*³² and other CPS studies.^{37,38} They afford a factorization of the high-dimensional coefficient tensor $C_{n_1 n_2 \dots n_M}$ into a product of nearest-neighbor 2-site correlator elements $C_{n_i n_j}^{[ij]}$,

$$|\Psi_{\text{CPS}}\rangle = \sum_{n_1 n_2 \dots n_M} \prod_{\langle ij \rangle} C_{n_i n_j}^{[ij]} |n_1 n_2 \dots n_M\rangle, \quad (4)$$

where $\langle ij \rangle$ indicates that only neighboring sites are taken into account. The correlators are represented by the second order tensors $\mathbf{C}^{[ij]}$,

$$\mathbf{C}^{[ij]} \equiv \begin{bmatrix} C_{00}^{[ij]} & C_{01}^{[ij]} \\ C_{10}^{[ij]} & C_{11}^{[ij]} \end{bmatrix}, \quad (5)$$

for each pair of neighboring spin orbitals i and j .

2.2.1 2-site Correlator Ansatz

We extended³³ the nearest-neighbors ansatz to *all* possible 2-site correlators,

$$|\Psi_{\text{CGTNS}}^{2s}\rangle = \sum_{n_1 n_2 \dots n_M} \prod_{i \leq j} C_{n_i n_j}^{[ij]} |n_1 n_2 \dots n_M\rangle, \quad (6)$$

which we therefore denoted Complete Graph Tensor Network States (CGTNS). Note that the notation for the CGTNS ansatz in Eq. (7) is different from the one presented in the original paper³³ in order to better discriminate the different tensor networks explored in this work. The total number of correlators in this ansatz is equal to $1/2M(M+1)$. Taking into account that each correlator is represented by a tensor of second order, Eq. (5) with q^2 elements ($q = 2$ for spin orbitals and $q = 4$ for spatial orbitals), the total number of variational parameters is equal to $1/2M(M+1)q^2$.

It is possible to avoid correlator matrices in CGTNS corresponding to interactions of certain sites with themselves — which we may call self-interaction (*si*) correlators — $C^{[ii]}$ — and to obtain the following ansatz

$$|\Psi_{\text{CGTNS}}^{2s/si}\rangle = \sum_{n_1 n_2 \dots n_M} \prod_{i < j} C_{n_i n_j}^{[ij]} |n_1 n_2 \dots n_M\rangle. \quad (7)$$

This removes M *si* correlators from the ansatz [$1/2M(M-1)$ correlators] without serious loss in accuracy as we shall demonstrate in Section 4.2. The graphical representation of such a tensor network ansatz at the example of a four-site system is shown in Figure 1 a).

Note that the CGTNS ansatz is related not only to TPVA, SBS, EPS, and CPS, but also to the Antisymmetric Products of Nonorthogonal Geminals ansatz.^{39,40} The latter may be considered as a special case of $|\Psi_{\text{CGTNS}}^{2s}\rangle$ where only the correlators between spin orbitals with the same spatial part are employed.

2.2.2 3-site Correlator Ansatz

CGTNS is an approximation to a CAS configuration interaction (CAS-CI) wave function, *i.e.*, to FCI in a restricted orbital space. Higher accuracy can be achieved by introducing higher-order correlators.³² For example, one may choose a tensor network

of 3-site correlators,

$$|\Psi_{\text{CGTNS}}^{3s}\rangle = \sum_{n_1 n_2 \dots n_M} \prod_{i < j < k} C_{n_i n_j n_k}^{[ijk]} |n_1 n_2 \dots n_M\rangle, \quad (8)$$

where $\mathbf{C}^{[ijk]}$ is the third-order tensor

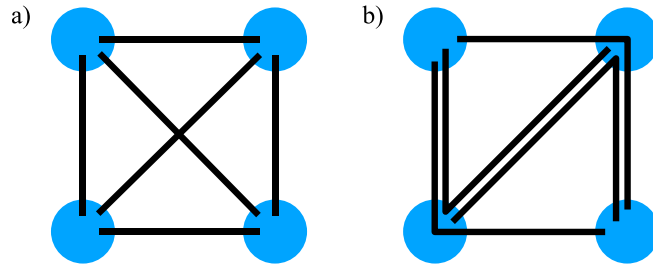
$$\mathbf{C}^{[ijk]} \equiv \begin{bmatrix} & & C_{001}^{[ijk]} & \text{---} & C_{011}^{[ijk]} \\ & C_{000}^{[ijk]} & \text{---} & C_{010}^{[ijk]} & \\ & & C_{101}^{[ijk]} & \text{---} & C_{111}^{[ijk]} \\ C_{100}^{[ijk]} & \text{---} & C_{110}^{[ijk]} & & \end{bmatrix}. \quad (9)$$

In the limit of M -site correlators the coefficients of Eq. (1), $C_{n_1 n_2 \dots n_M}$, are recovered. In a 3-site correlator ansatz the total number of correlators (third-order tensors) is $1/6M(M+1)(M+2)$. As the tensor of third order, $\mathbf{C}^{[ijk]}$ of Eq. (9), has q^3 elements, this yields $1/6M(M+1)(M+2)q^3$ variational degrees of freedom. In analogy to the case of second-order tensors, one can remove *si* tensors of the type $\mathbf{C}^{[iii]}$, $\mathbf{C}^{[iik]}$, and $\mathbf{C}^{[ikk]}$ to obtain

$$|\Psi_{\text{CGTNS}}^{3s/si}\rangle = \sum_{n_1 n_2 \dots n_M} \prod_{i < j < k} C_{n_i n_j n_k}^{[ijk]} |n_1 n_2 \dots n_M\rangle, \quad (10)$$

which removes M^2 correlators. A graphical representation of such a tensor network is shown in Figure 1 b). As will be shown in Sections 4.2 and 4.3, *si* correlators do *not* play a negligible role in the 3-site correlator ansatz in contrast to their 2-site correlator analogs.

Figure 1: Graphical representations of the a) $\Psi_{\text{CGTNS}}^{2s/si}$ and b) $\Psi_{\text{CGTNS}}^{3s/si}$ ansätze for a system containing four sites. The blue vertices represent sites, while the connecting black lines represent correlators.



2.2.3 Hybrid 2-Site and 3-Site Correlator Ansätze

For better optimization efficiency, correlators can be introduced and optimized gradually starting with 2-site correlators and continuing with 3-site correlators. Having first optimized 2-site correlators, we may freeze their values and start the optimization of 3-site correlators incorporated in the ansatz as scaling factors

$$\left| \Psi_{\text{CGTNS}}^{3s[2s]} \right\rangle = \sum_{n_1 n_2 \dots n_M} \underbrace{\prod_{i \leq j} C_{n_i n_j}^{[ij]}}_{\text{frozen}} \underbrace{\prod_{k < l < m} C_{n_k n_l n_m}^{[klm]}}_{\text{active}} |n_1 n_2 \dots n_M\rangle, \quad (11)$$

or in self-interaction free form

$$\left| \Psi_{\text{CGTNS}}^{3s/si[2s]} \right\rangle = \sum_{n_1 n_2 \dots n_M} \underbrace{\prod_{i \leq j} C_{n_i n_j}^{[ij]}}_{\text{frozen}} \underbrace{\prod_{k < l < m} C_{n_k n_l n_m}^{[klm]}}_{\text{active}} |n_1 n_2 \dots n_M\rangle. \quad (12)$$

However, introduction of products of 2-site and 3-site correlators will augment the non-linear structure of the CGTNS ansatz, which in turn could hamper the convergence of the optimization and increase the probability of getting trapped in local minima. This problem could be alleviated by splitting up the hybrid ansatz into a *sum* of 2-site correlator and 3-site correlator products

$$\left| \Psi_{\text{CGTNS}}^{3s+[2s]} \right\rangle = \sum_{n_1 n_2 \dots n_M} \left[\underbrace{\prod_{i \leq j} C_{n_i n_j}^{[ij]}}_{\text{frozen}} + \underbrace{\prod_{k < l < m} C_{n_k n_l n_m}^{[klm]}}_{\text{active}} \right] |n_1 n_2 \dots n_M\rangle, \quad (13)$$

or in self-interaction free form

$$\left| \Psi_{\text{CGTNS}}^{3s/si+[2s]} \right\rangle = \sum_{n_1 n_2 \dots n_M} \left[\underbrace{\prod_{i \leq j} C_{n_i n_j}^{[ij]}}_{\text{frozen}} + \underbrace{\prod_{k < l < m} C_{n_k n_l n_m}^{[klm]}}_{\text{active}} \right] |n_1 n_2 \dots n_M\rangle. \quad (14)$$

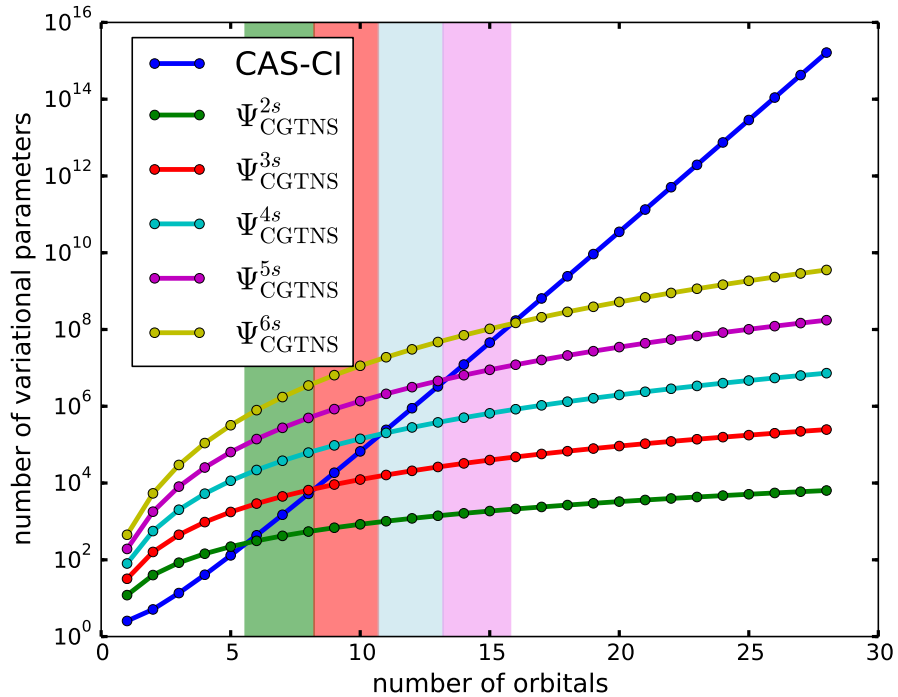
These parameterization strategies can be naturally continued to higher-order correlators. It is possible, but of no practical value, to finally include up to M -site correlators. Already four-site correlators will make the ansatz intractable, because of their sheer number. Hence, only the selective inclusion of higher-order correlators will be feasible. The number of variational parameters for all CGTNS variants depends only on the number of spin orbitals, M . By analogy to Ψ_{CGTNS}^{2s} and Ψ_{CGTNS}^{3s} , one can define the ansätze for 4-, 5-, 6-site *etc.* correlators to be denoted as Ψ_{CGTNS}^{4s} , Ψ_{CGTNS}^{5s} , Ψ_{CGTNS}^{6s} and so forth. Assuming that the number of electrons N is growing with the number of spatial orbitals, $M_{\text{orb}} = M/2$, and that they are equal, $N = M_{\text{orb}}$, we obtain for

the number of ONVs, N_{ONV} , with spin projection $M_s = 0$ for the active space of N electrons in M_{orb} orbitals denoted as $\text{CAS}(N, M_{\text{orb}})^{16}$

$$N_{\text{ONV}} = \frac{2}{\pi M_{\text{orb}}} 4^{M_{\text{orb}}}. \quad (15)$$

Note that if one exploits symmetry, this number can be decreased. The scaling of the number of variational parameters with respect to the number of orbitals for all variations of CGTNS as well as for CAS-based methods is shown in Figure 2.

Figure 2: Scaling of variational parameters in CAS-CI and various CGTNS parameterizations with increasing $\text{CAS}(N, M_{\text{orb}})$ sizes for a number of electrons N identical to the number of active spatial orbitals M_{orb} , $N = M_{\text{orb}}$. The colored shaded regions denote active spaces for which the low-order CGTNS ansatz of the same color introduces less variational parameters than the exact solution.



Clearly, one would stop the systematic extension of the CGTNS ansatz by higher-order correlators when the change in energy drops below a certain threshold. It would be most desirable to determine this threshold so that relative energies rather than absolute electronic energies are accurately approximated. The maximum number of variational parameters would then be determined by the highest-order tensor network ansatz. An alternative strategy is to introduce higher-order correlators at or before the

points where the curve corresponding to a specific CGTNS ansatz crosses the CAS-CI curve in Figure 2. The colored regions in Figure 2 show the scope of application for each CGTNS parameterization (the regions are marked with a color corresponding to the curve representing that CGTNS ansatz). Such a strategy, however, only gives a qualitative idea on the applicability of CGTNS schemes. A more rigorous way will be developed in Section 4.4.

The set of higher-order correlators can inflate the variational space to that of CAS-CI and beyond (the regions where curves corresponding to CGTNS ansätze are above the CAS line in Figure 2). To properly cope with such situations requires to introduce higher-order correlators only for certain sites which may be determined based on entanglement measures. The entanglement between sites can be estimated from single-orbital entropies and mutual information entropies^{41,42,43,44,45} obtained for the low-order correlators such as those in Ψ_{CGTNS}^{2s} . In this, work such an ansatz will be denoted as $\Psi_{\text{CGTNS}}^{3s[2s]\text{sel}}$.

2.3 The Spin-Adapted CGTNS Ansatz

The expectation value of the Hamiltonian operator over an approximate N -electron wave function Ψ_{CGTNS} is an upper bound to the exact CAS-CI reference energy,

$$E_{\text{CAS-CI}} = \frac{\langle \Psi_{\text{CAS-CI}} | H | \Psi_{\text{CAS-CI}} \rangle}{\langle \Psi_{\text{CAS-CI}} | \Psi_{\text{CAS-CI}} \rangle} \leq \frac{\langle \Psi_{\text{CGTNS}} | H | \Psi_{\text{CGTNS}} \rangle}{\langle \Psi_{\text{CGTNS}} | \Psi_{\text{CGTNS}} \rangle}, \quad (16)$$

where for Ψ_{CGTNS} we can have any approximation introduced above (Ψ_{CGTNS}^{2s} , Ψ_{CGTNS}^{3s} , $\Psi_{\text{CGTNS}}^{2s/si}$, $\Psi_{\text{CGTNS}}^{3s/si}$, $\Psi_{\text{CGTNS}}^{3s/si[2s]}$, $\Psi_{\text{CGTNS}}^{3s[2s]\text{sel}}$). For a specific ONV $|t\rangle = |t_1 t_2 \dots t_M\rangle$ in the Ψ_{CGTNS}^{2s} ansatz, for instance, we approximate a CI coefficient $C_t = C_{t_1 t_2 \dots t_M}$ as,

$$C_t \approx C_t^{\text{CGTNS}} = \langle t | \Psi_{\text{CGTNS}} \rangle = \prod_{i \leq j} C_{n_i n_j}^{[ij]}, \quad \forall n_i, n_j \in |t\rangle, \quad (17)$$

so that the CGTNS wave function can be rewritten in compact form as

$$|\Psi_{\text{CGTNS}}\rangle = \sum_n C_n^{\text{CGTNS}} |n\rangle. \quad (18)$$

Then, the normalization condition reads

$$\begin{aligned} \langle \Psi_{\text{CGTNS}} | \Psi_{\text{CGTNS}} \rangle &= \sum_{nl} (C_n^{\text{CGTNS}})^* C_l^{\text{CGTNS}} \langle n | l \rangle \\ &= \sum_{nl} (C_n^{\text{CGTNS}})^* C_l^{\text{CGTNS}} \delta_{nl} = \sum_n (C_n^{\text{CGTNS}})^2. \end{aligned} \quad (19)$$

Accurate calculations demand spin-adapted configuration state functions (CSFs),

$$|\Phi_p^{\text{CSF}}\rangle = \sum_n K_{pn} |n\rangle, \quad (20)$$

where K_{pn} are Clebsch–Gordan coefficients generating these spin-adapted basis functions. The CAS-CI function can then be expanded as

$$|\Psi_{\text{CAS-CI}}\rangle = \sum_p S_p |\Phi_p^{\text{CSF}}\rangle. \quad (21)$$

Since Clebsch–Gordan coefficients K_{pn} from Eq. (20) are fixed, one can no longer optimize the weights of Slater determinants, C_n^{CGTNS} , and the straightforward CGTNS concept breaks down. However, it is possible to approximate S_p in the previous equation as a sum of Clebsch–Gordan coefficients K_{pn} scaled by C_n^{CGTNS} for every $|n\rangle$ in Eq. (20),

$$S_p \approx S_p^{\text{CGTNS}} = \sum_n K_{pn} C_n^{\text{CGTNS}}. \quad (22)$$

With the weights S_p^{CGTNS} in Eq. (22), we define the spin-adapted CGTNS ansatz as

$$|\Psi_{\text{CGTNS}}\rangle = \sum_p \sum_n K_{pn} C_n^{\text{CGTNS}} |\Phi_p^{\text{CSF}}\rangle = \sum_p S_p^{\text{CGTNS}} |\Phi_p^{\text{CSF}}\rangle. \quad (23)$$

The normalization will then take the following form

$$\begin{aligned} \langle \Psi_{\text{CGTNS}} | \Psi_{\text{CGTNS}} \rangle &= \sum_{pn} \sum_{ql} S_p^{\text{CGTNS}} K_{pn} S_q^{\text{CGTNS}} K_{ql} \langle n | l \rangle \\ &= \sum_{pn} \sum_{ql} S_p^{\text{CGTNS}} K_{pn} S_q^{\text{CGTNS}} K_{ql} \delta_{nl} \\ &= \sum_{pq} S_p^{\text{CGTNS}} S_q^{\text{CGTNS}} \sum_n K_{pn} K_{qn}, \end{aligned} \quad (24)$$

where we assume real coefficients S_p^{CGTNS} and K_{pn} . In the following, we will always consider spin-adapted CGTNS parameterizations.

2.4 Monte Carlo Optimization

The highly nonlinear dependence of the CGTNS ansatz on correlators makes convergence of optimization procedures toward a global minimum a difficult task. Hence, we continue to employ a variational Monte Carlo optimization scheme.^{33,46} With Eqs. (23) and (24), the expectation value of the Hamiltonian for a CGTNS wave function reads

$$E_{\text{CGTNS}} = \frac{\sum_r S_r^{\text{CGTNS}} \langle \Psi_{\text{CGTNS}} | H | \Phi_r^{\text{CSF}} \rangle}{\sum_{pq} S_p^{\text{CGTNS}} S_q^{\text{CGTNS}} \sum_n K_{pn} K_{qn}}. \quad (25)$$

We can rewrite Eq. (25) in a more useful form for Monte Carlo sampling,

$$E_{\text{CGTNS}} = \frac{\sum_r (S_r^{\text{CGTNS}})^2 \frac{\langle \Psi_{\text{CGTNS}} | H | \Phi_r^{\text{CSF}} \rangle}{S_r^{\text{CGTNS}}}}{\sum_{pq} S_p^{\text{CGTNS}} S_q^{\text{CGTNS}} \sum_n K_{pn} K_{qn}}, \quad (26)$$

where the $(S_r^{\text{CGTNS}})^2$ represent strictly non-negative probabilities for corresponding energy estimators

$$E_r = \frac{\langle \Psi_{\text{CGTNS}} | H | \Phi_r^{\text{CSF}} \rangle}{S_r^{\text{CGTNS}}} = \sum_s \frac{S_s^{\text{CGTNS}}}{S_r^{\text{CGTNS}}} \langle \Phi_s^{\text{CSF}} | H | \Phi_r^{\text{CSF}} \rangle. \quad (27)$$

Since every S_s^{CGTNS} is determined by a set of correlators $\tilde{\mathbf{C}}$, with $\tilde{\mathbf{C}} = \{\mathbf{C}^{[11]}, \mathbf{C}^{[12]}, \dots, \mathbf{C}^{[ij]}, \dots, \mathbf{C}^{[NM]}\}$ through Eqs. (17) and (22) for the 2-site case, for every choice of correlators $\tilde{\mathbf{C}}$ one can assign an energy $E_r(\tilde{\mathbf{C}})$

$$E_r(\tilde{\mathbf{C}}) = \sum_s \frac{S_s^{\text{CGTNS}}(\tilde{\mathbf{C}})}{S_r^{\text{CGTNS}}(\tilde{\mathbf{C}})} \langle \Phi_s^{\text{CSF}} | H | \Phi_r^{\text{CSF}} \rangle. \quad (28)$$

Introducing an artificial temperature T (a parameter with the dimension of energy, measured in Hartree), it is possible to sample the continuous variables $\tilde{\mathbf{C}}$ following a canonical ensemble with the weight of a configuration given by $\exp[-E_r(\tilde{\mathbf{C}})/T]$. The limit $T \rightarrow 0$ Hartree yields the desired ground state of the molecule. The optimization procedure can be easily controlled by tuning T . To avoid getting trapped in local minima, the parallel tempering scheme is applied³³ during the optimization with swap-move probabilities between two neighboring temperatures defined as

$$p((T_i, E_i) \leftrightarrow (T_{i+1}, E_{i+1})) = \min\{1, \exp(\Delta E/\Delta T)\}, \quad (29)$$

where $\Delta E = E_{i+1} - E_i$ and $\Delta T = T_{i+1}T_i/(T_i - T_{i+1})$. The set of P temperatures in the range $[T_1, T_P]$ are chosen according to the formula

$$T_l = T_1 \left(\exp \frac{\ln T_P - \ln T_1}{P - 1} \right)^{l-1}, \quad \text{with } l = 1 \dots P. \quad (30)$$

It is clear from Eq. (28) that this procedure will only be feasible for large CAS if not all Φ_r^{CSF} are required. The exponential scaling of the dimension of the Hilbert space with the number of orbitals is clearly a restriction of the CGTNS approach which it shares with the FCI Quantum Monte Carlo approach of Alavi and co-workers.^{47, 48, 49} Accordingly, CSFs that hardly contribute to the energy must be omitted.

2.4.1 Gradient-based Optimization

The Monte Carlo optimized CGTNS ansatz, *e.g.* Ψ_{CGTNS}^{2s} , can be taken as a starting point for a non-stochastic local optimization for refinement. The local gradient

$$\nabla E_{\text{CGTNS}} = \left(\frac{\partial E_{\text{CGTNS}}}{\partial C_{00}^{[11]}}, \frac{\partial E_{\text{CGTNS}}}{\partial C_{01}^{[11]}}, \frac{\partial E_{\text{CGTNS}}}{\partial C_{10}^{[11]}}, \frac{\partial E_{\text{CGTNS}}}{\partial C_{11}^{[11]}}, \dots, \frac{\partial E_{\text{CGTNS}}}{\partial C_{11}^{[MM]}} \right), \quad (31)$$

can be evaluated and exploited in such a local search. Introducing the correlators together with the corresponding gradient, Eq. (31), into the Quasi-Newton optimization method with the Broyden-Fletcher-Goldfarb-Shanno algorithm for an update of the Hessian matrix,⁵⁰ we can further lower the CGTNS energy. An alternative way is to consider only the gradient of the CGTNS energy for the correlators corresponding to certain pairs of sites i and j at a time

$$\nabla^{[ij]} E_{\text{CGTNS}} = \left(\frac{\partial E_{\text{CGTNS}}}{\partial C_{00}^{[ij]}}, \frac{\partial E_{\text{CGTNS}}}{\partial C_{01}^{[ij]}}, \frac{\partial E_{\text{CGTNS}}}{\partial C_{10}^{[ij]}}, \frac{\partial E_{\text{CGTNS}}}{\partial C_{11}^{[ij]}} \right). \quad (32)$$

Switching between all possible pairs of the sites in the CGTNS ansatz, convergence should be reached at some point. We will refer to the first optimization strategy as a gradient optimization, while the second strategy will be denoted “reduced” gradient optimization in the following. Following Chan and coworkers,³² we note that, because the wave function is linear with respect to correlators of a given set of sites, the components of the gradient for the chosen correlator may define a vector space for the optimization. Hence, it is possible to introduce the Hamiltonian and overlap matrix in the vector space spanned by the components of the local gradient.³² Finding the eigenpairs corresponding to this Hamiltonian and switching between all possible pairs, we may finally obtain the same solution as in the case of “reduced” gradient optimization.

3 Computational Details

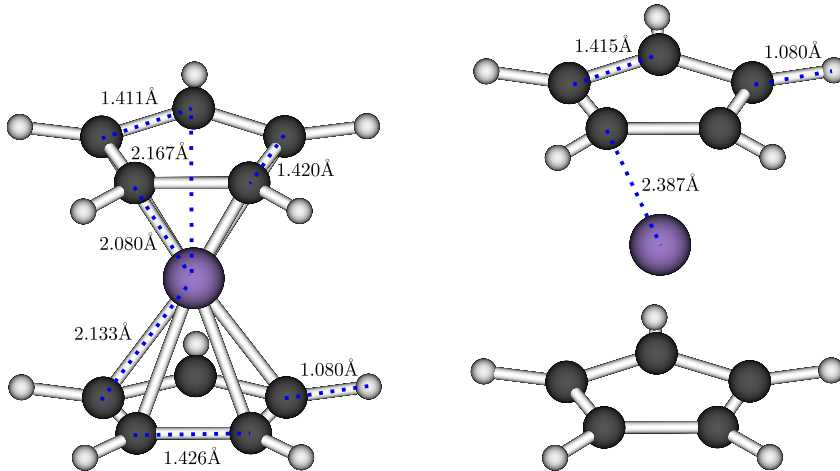
A suitable molecule for the analysis of the various CGTNS parameterizations should have a strong multi-configurational character. Manganocene is such a molecule. It is particularly interesting because most DFT calculations fail to predict the proper ground spin state.⁵¹ While it is decisive to be able to predict the energy difference between high- and low-spin states in transition metal compounds, it turned out to be hard to predict the energy difference between sextet and doublet state in manganocene.⁵¹ Satisfactory accuracy can be achieved by describing these two spin states with the

CASPT2 method.⁵² Phung *et al.* showed⁵² that dynamic electron correlation is as important as static electron correlation for the quantitative prediction of the spin state splitting (see also Ref. 53 for an in-depth discussion). Our CGTNS ansatz operates in an active space of selected orbitals and hence approximates a CAS-CI wave function. While this is no issue for the analysis of the CGTNS parameterizations, reliable predictions will require to consider dynamic correlation, which can, for instance, be included by short-range DFT.^{54,23} Hence, the theoretical reference for our study will be the CAS-SCF result rather than the CASPT2 data by Phung *et al.*⁵²

Density Functional Theory (DFT) structure optimizations of manganocene were conducted with the TURBOMOLE program version 6.5^{55,56} in the doublet and sextet states. The hybrid Perdew–Burke–Ernzerhof (PBE0)⁵⁷ density functional together with triple- ζ valence polarized (def2-TZVP)⁵⁸ (for carbon and hydrogen atoms) and quadruple- ζ valence polarized (def2-QZVPP)⁵⁹ (for the manganese atom) basis sets were chosen. In addition, single-point DFT calculations were performed for the sextet and doublet states with the pure Perdew–Burke–Ernzerhof (PBE)⁶⁰ density functional. Note, that for all DFT calculations Grimme D3 dispersion corrections⁶¹ and the second-order scalar-relativistic Douglas-Kroll-Hess Hamiltonian^{62,63,64,65} were switched on.

The doublet and sextet manganocene structures were optimized with DFT-PBE0-D3 in C_{2v} and D_{5h} symmetries, respectively. These optimized structures were then taken for all single-point calculations in this work; see Figure 3.

Figure 3: The PBE0-D3/def2-TZVP(C,H)/def2-QZVPP(Mn) structures of manganocene in the doublet state (left) and the sextet state (right). Hydrogen atoms in white, carbon atoms in black, and manganese atoms in purple.



All reference CAS-SCF calculations were performed with the MOLCAS 8.1 package.¹⁶ The extended ANO-RCC basis sets (with a total of 1487 basis functions) were employed with [6s4p3d1f] contraction for hydrogen,⁶⁶ [8s8p4d3f2g] contraction for carbon,⁶⁷ and [10s9p8d6f4g2h] contraction for manganese.⁶⁸ Two-electron integrals were approximated with a Cholesky decomposition technique⁶⁹ using a threshold of 10^{-6} Hartree. Also in these calculations, the second-order scalar-relativistic Douglas–Kroll–Hess Hamiltonian^{62,63,64,70} was chosen.

The CGTNS program reads one- and two-electron molecular orbital integrals for the second-quantized electronic Hamiltonian generated by MOLCAS. The integrals are calculated from the natural orbitals of the corresponding CAS-SCF reference calculations. For the CGTNS calculations we improved on our original implementation presented in Ref. 33. The gradient optimization and the “reduced” gradient optimization according to Eq. (31) and Eq. (32), respectively (see Section 2.4.1), were implemented. In addition to the existing Ψ_{CGTNS}^{2s} ansatz, we implemented $\Psi_{\text{CGTNS}}^{2s/si}$, Ψ_{CGTNS}^{3s} , $\Psi_{\text{CGTNS}}^{3s/si}$, $\Psi_{\text{CGTNS}}^{3s[2s]}$, $\Psi_{\text{CGTNS}}^{3s+[2s]}$, $\Psi_{\text{CGTNS}}^{3s/si[2s]}$, and $\Psi_{\text{CGTNS}}^{3s/si+[2s]}$.

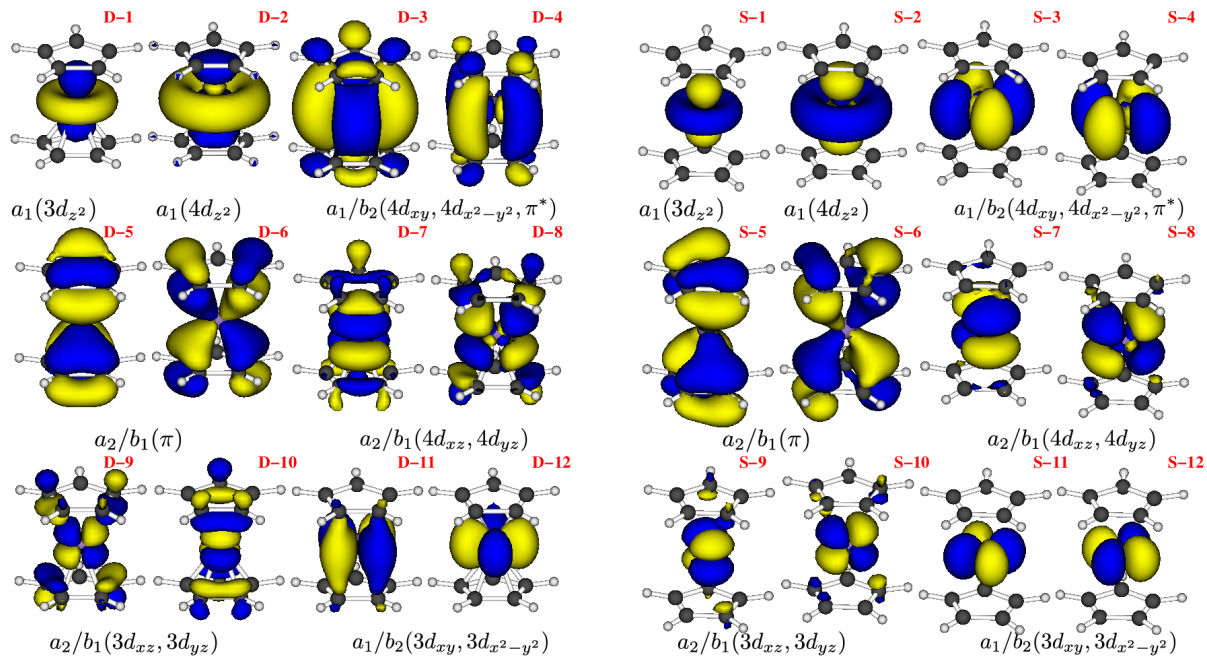
The $\Psi_{\text{CGTNS}}^{3s[2s]\text{sel}}$ ansatz is a slightly modified version of the $\Psi_{\text{CGTNS}}^{3s[2s]}$ parameterization. In contrast to $\Psi_{\text{CGTNS}}^{3s[2s]}$, it contains the 3-site correlators corresponding only to the most entangled spin orbitals (the same holds true for $\Psi_{\text{CGTNS}}^{3s+[2s]\text{sel}}$ and $\Psi_{\text{CGTNS}}^{3s+[2s]}$). Ideally, these selected spin orbitals should be chosen using entanglement measure based on the single-orbital entropies and the mutual information.^{41,42,43,44,45} However, here we select 3-site correlators for spin orbitals corresponding to spatial orbitals with natural orbital occupation numbers in the range [0.02, 1.98] (unless otherwise noted). This follows the Unrestricted Natural Orbital-CAS (UNO-CAS) model,^{71,72} in which the active space is constructed from Unrestricted Hartree–Fock (UHF) natural (spatial) orbitals with occupation numbers between 0.02 and 1.98. The same strategy was also adopted for choosing an active space in DMRG calculations.⁷³ UHF natural orbitals may even represent a good choice for the orbital basis.^{71,72,73}

4 Discussion

4.1 Reference CAS-SCF(9,12) Energy Difference

The CAS-SCF(9,12) reference calculations for both spin states in C_{2v} symmetry were carried out for active orbital spaces proposed in Ref. 52. The orbitals included into the active spaces of the CAS-SCF calculation are shown in Figure 4.

Figure 4: Converged natural orbitals — denoted as **D-i** and **S-i** (in red color) for the doublet and sextet states, respectively ($\mathbf{i} = \{1, 2, 3, \dots, 12\}$) — that constitute the active spaces in the CAS-SCF(9,12) reference calculations of manganocene.



Note that an active space consisting of 9 electrons in 12 spatial orbitals chosen according to Ref. 52 turned out to be not without difficulties. In particular, for both spin states one cannot obtain pure π^* orbitals without the inclusion of lower lying π orbitals, high lying π^* orbitals, and $4d_{xy}/4d_{x^2-y^2}$ orbitals into the active space. This would introduce two additional electrons and six additional orbitals into active space. Moreover, symmetry breaking may occur for the sextet state. Nevertheless, in order to be in line with Ref. 52, we adopt the smaller active space from that reference as the choice of the active space is of little importance for our wave-function parameterization analysis. The natural orbitals produced in the CAS-SCF(9,12) calculation were then chosen for the CGTNS calculations. Hence, the CGTNS result approximates the CAS-SCF(9,12) result.

The reference energy difference calculated with CAS-SCF(9,12) for the sextet and doublet states is presented in Table I. The CAS-SCF(9,12) energy difference of -40.59 kcal/mol, deviates from the experimental value of 3.58 kcal/mol because of the lack of dynamic electron correlation. The PBE0 result of -8.28 kcal/mol (see DFT-PBE0-D3 in Table I) is much closer to the experimental result, but fails to predict the correct

sign. PBE (see DFT-PBE-D3 in Table I), predicts the correct sign, but the energy is overestimated by approximately 19 kcal/mol. The CASPT2 energy difference (see CASPT2 in Table I) is very close to the experimental result.⁵² We emphasize again that, in this work, we concentrate on the assessment of static correlation described by tensor network parameterizations. Dynamic correlation may be included through second order perturbation theory^{74,75} or short-range DFT methods.^{54,23}

Table I: Electronic energy difference (in kcal/mol) of manganocene in the sextet $E[{}^6A_1]$ and doublet $E[{}^2A_1]$ states, $E[{}^6A_1] - E[{}^2A_1]$ obtained for different methods described in Section 3. CASPT2 and experimental (exp.) results were taken from Ref. 52.

	DFT-PBE-D3	DFT-PBE0-D3	CAS-SCF(9,12)	CASPT2	exp.
$E[{}^6A_1] - E[{}^2A_1]$	22.55	-8.28	-40.59	5.77	3.58

4.2 Manganocene — Sextet State

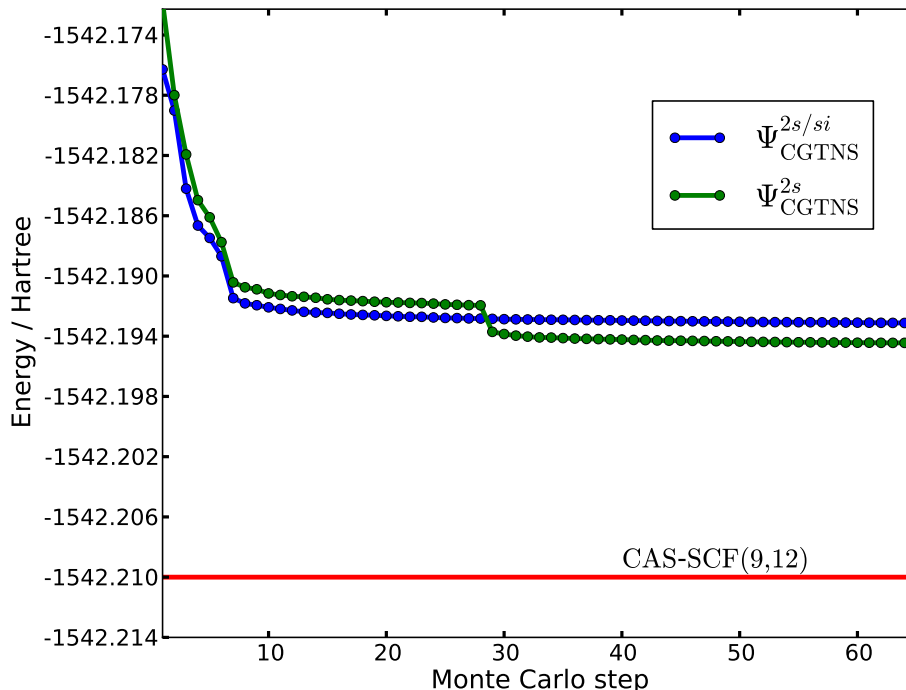
13108 ONVs span the configurational space corresponding to an active space of 9 electrons in 12 spatial orbitals (see Figure 4) for the sextet state of manganocene in C_{2v} point group symmetry. The number of CGTNS variational parameters for 24 spin orbitals is 1200 for Ψ_{CGTNS}^{2s} and 1104 for $\Psi_{\text{CGTNS}}^{2s/si}$. Hence, the parameterization in Ψ_{CGTNS}^{2s} and $\Psi_{\text{CGTNS}}^{2s/si}$ reduce the variational space by more than 90% in both cases, see Table II. The number of spin-adapted CSFs for the sextet state is 11628 and therefore not much lower than the total number of ONVs so that the CGTNS reduction is still approximately 90%. At the same time, the deviation of the CGTNS energy from the reference energy is lower than 20 mHartree, see Table II.

Table II: Electronic energies for the sextet state of manganocene. A positive/negative percentage indicates a decreased/increased parameter space compared to the 13108 CI coefficients in the CAS-SCF(9,12) reference calculation.

parameterization	parameters	percentage	energy/Hartree
CAS-SCF(9,12)	13108		-1542.209620
Ψ_{CGTNS}^{2s}	1200	91%	-1542.194072
$\Psi_{\text{CGTNS}}^{2s/si}$	1104	92%	-1542.192755
$\Psi_{\text{CGTNS}}^{3s/si}$	16192	-29%	-1542.195739
Ψ_{CGTNS}^{3s}	20800	-59%	-1542.197777
$\Psi_{\text{CGTNS}}^{3s/si[2s]}$	16192	-29%	-1542.195415
$\Psi_{\text{CGTNS}}^{3s/si+[2s]}$	16192	-29%	-1542.195290
$\Psi_{\text{CGTNS}}^{3s[2s]}$	20800	-59%	-1542.195283
$\Psi_{\text{CGTNS}}^{3s+[2s]}$	20800	-59%	-1542.195227
$\Psi_{\text{CGTNS}}^{3s[2s]\text{sel}}$	4480	66%	-1542.194826
$\Psi_{\text{CGTNS}}^{3s+[2s]\text{sel}}$	4480	66%	-1542.194822

Note that the Ψ_{CGTNS}^{2s} parameterization is slightly more accurate than the $\Psi_{\text{CGTNS}}^{2s/si}$ parameterization yielding a 0.001317 Hartree lower energy, induced by only 96 additional variational parameters. The convergence behavior of both parameterization is similar, see Figure 5. The Monte Carlo optimizations for both CGTNS parameterizations have reached convergence. However, the Monte Carlo sampling of CGTNS parameters requires significantly more computational time than the traditional diagonalization approach. Hence, the CGTNS ansatz will be beneficial only for cases where exact diagonalization is no longer feasible.

Figure 5: Convergence behavior of Ψ_{CGTNS}^{2s} and $\Psi_{\text{CGTNS}}^{2s/si}$ parameterizations for manganocene in the lowest sextet state.



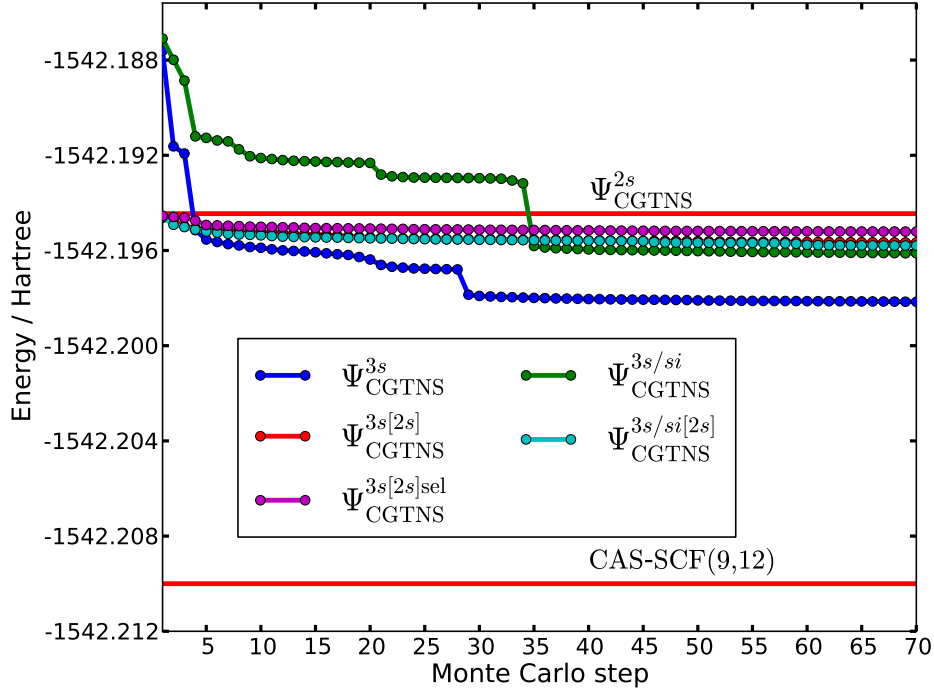
As the 2-site correlator CGTNS energy deviates from the CAS-SCF reference, it is important to analyze whether 3-site correlators better approximate the reference result. The 3-site correlator variants of CGTNS $\Psi_{\text{CGTNS}}^{3s}/\Psi_{\text{CGTNS}}^{3s[2s]}$ and $\Psi_{\text{CGTNS}}^{3s/si}/\Psi_{\text{CGTNS}}^{3s/si[2s]}$ dramatically increase the variational space from 1200 to 20800 and 16192 parameters, respectively (see Table II). Hence, it is inevitable to include only those 3-site correlators of the most entangled spin orbitals. According to the selection criterion described in Section 3, we have chosen the natural orbitals **S-1**, **S-9**, **S-10**, **S-11**, **S-12**, see Figure 4. The additional 3-site correlators were constructed for 10 spin orbitals attributed to the selected natural orbitals, which resulted in a total of 1760 variational parameters for the hybrid CGTNS ansatz $\Psi_{\text{CGTNS}}^{3s[2s]\text{sel}}$. With this parameterization the energy converges very fast, but lowers it by only -0.272 mHartree.

If additional 3-site correlators are constructed considering also orbitals **S-5** and **S-6** (Figure 4) that feature occupation numbers larger than 1.98 (i.e., 1.99 and larger), a total of 4480 variational parameters results. In this case, the energy is lowered by 0.754 mHartree, see Table II and Figure 6. In order to understand the reason for this small effect, we compare to the other 3-site correlator CGTNS parameterizations. One

can understand from Table II that the lowest energy, -1542.197777 Hartree, is obtained with the Ψ_{CGTNS}^{3s} ansatz (the error is -11.843 mHartree), while the least accurate energy, -1542.195283 Hartree, is obtained from the $\Psi_{\text{CGTNS}}^{3s[2s]}$ ansatz. Note that in the best case the energy is lowered by only -0.003705 Hartree, which is lower by -0.002951 Hartree compared to the energy from $\Psi_{\text{CGTNS}}^{3s[2s]\text{sel}}$. And if one compares the energy from $\Psi_{\text{CGTNS}}^{3s[2s]\text{sel}}$ to the conceptually similar ansatz $\Psi_{\text{CGTNS}}^{3s[2s]}$, the difference is -0.000457 Hartree, which is rather small. Hence, although 3-site correlators do not significantly improve on the total electronic energy, the $\Psi_{\text{CGTNS}}^{3s[2s]\text{sel}}$ ansatz is a good approximation to $\Psi_{\text{CGTNS}}^{3s[2s]}$.

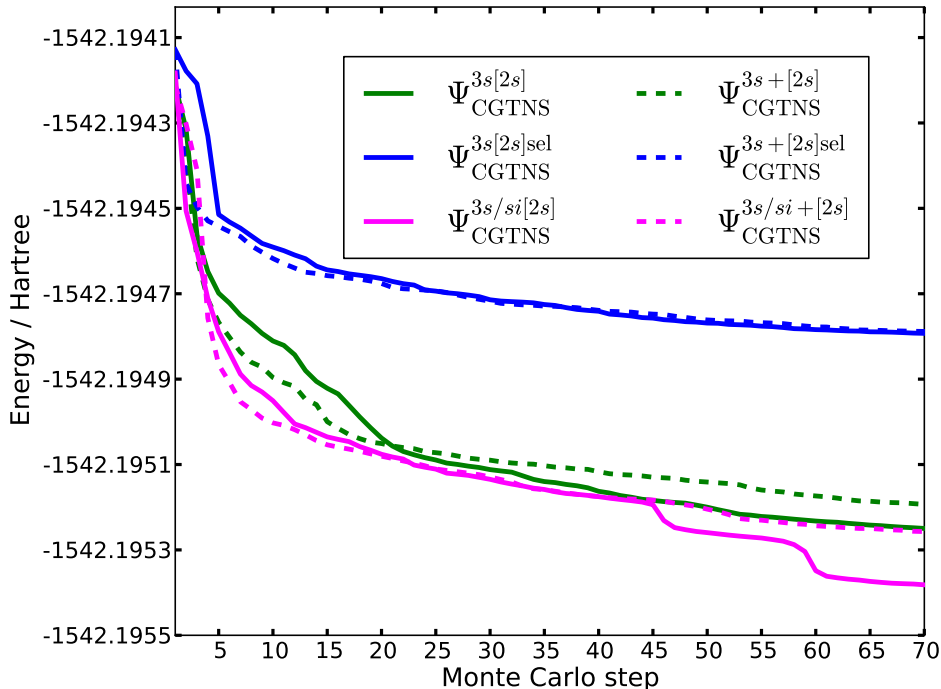
If all *si* correlators are omitted, the $\Psi_{\text{CGTNS}}^{3s/si}$ ansatz will minimize the energy to -1542.195739 Hartree, while $\Psi_{\text{CGTNS}}^{3s/si[2s]}$ yields a slightly higher energy of -1542.195415 Hartree. In both cases, the hybrid ansätze give higher energies than those from pure 3-site correlator schemes. We note that $\Psi_{\text{CGTNS}}^{3s/si[2s]}$ is somewhat lower in energy than $\Psi_{\text{CGTNS}}^{3s[2s]}$, while Ψ_{CGTNS}^{3s} is far lower than $\Psi_{\text{CGTNS}}^{3s/si}$. The Monte Carlo parallel tempering optimization procedure fails to decrease the error by more than -0.01 Hartree, even though the 3-site correlator schemes have much more variational parameters than CAS-SCF. Obviously, the CGTNS ansatz introduces a highly non-linear parameterization which requires non-trivial optimization techniques to avoid local minima. Various temperature sets were used for the Monte Carlo parallel tempering optimization and only best results are reported in this work. The convergence behavior for all parameterizations is shown in Figure 6. One of the problems are rare swap moves between neighboring temperatures. If the temperature set has a smaller step, many swaps occur, but this is equivalent to performing simulations on similar sets. For the hybrid parameterizations the parallel tempering scheme does not work well because the energies resulting from every temperature set are biased to the already optimized Ψ_{CGTNS}^{2s} correlators. This, in turn, increases ΔE between the neighboring temperatures and the swap moves are not likely to appear, see Eq. (29). This can be easily seen from the convergence curves in Figure 6, where we observe steep steps for Ψ_{CGTNS}^{3s} and $\Psi_{\text{CGTNS}}^{3s/si}$, while all the hybrid parameterizations show a smooth convergence behavior. A solution might be to use dynamically optimized temperatures.⁷⁶ However, the accuracy achieved here is sufficient for the analysis of CGTNS parameterizations. We emphasize that accurate relative energies are the ultimate target for processes in low energy chemical physics.

Figure 6: Convergence behavior of 3-site correlator CGTNS parameterizations for manganocene in the lowest-energy sextet state.



In addition, calculations employing alternative $\Psi_{\text{CGTNS}}^{3s+[2s]}$, $\Psi_{\text{CGTNS}}^{3s/si+[2s]}$, and $\Psi_{\text{CGTNS}}^{3s+[2s]sel}$ hybrid parameterizations were performed. One can see from Table II that the final energies calculated from $\Psi_{\text{CGTNS}}^{3s+[2s]}$, $\Psi_{\text{CGTNS}}^{3s/si+[2s]}$, and $\Psi_{\text{CGTNS}}^{3s+[2s]sel}$ wave functions are slightly higher than those of the corresponding $\Psi_{\text{CGTNS}}^{3s[2s]}$, $\Psi_{\text{CGTNS}}^{3s/si[2s]}$, and $\Psi_{\text{CGTNS}}^{3s[2s]sel}$ parameterizations, respectively. In the case of $\Psi_{\text{CGTNS}}^{3s/si+[2s]}$, the energy is higher than the one from $\Psi_{\text{CGTNS}}^{3s/si[2s]}$ by only 0.125 mHartree, while in the other cases the difference is even smaller. The only advantage of the alternative hybrid schemes is slightly faster convergence which can be seen in Figure 7.

Figure 7: Convergence behavior of hybrid CGTNS parameterizations for manganocene in the lowest-energy sextet state.



If the (local) gradient optimization, Eq. (31), is applied after Monte Carlo optimization, the energy is decreased by only -0.34909 mHartree to -1542.19442146 Hartree. With the “reduced” gradient optimization, Eq. (32), the result deteriorates. The same holds true for the variational optimization suggested by Changlani *et al.* in their work on CPS ansatz³² when applied for CGTNS ansatz. Apparently, while such a variational optimization works well in the case of CPS ansatz,³² the presence of correlators different from the ones corresponding to the nearest neighbors introduces unsurmountable difficulties.

4.3 Manganocene — Doublet State

The configurational space of the doublet state is spanned by 98060 ONVs in C_{2v} point group symmetry for an active space consisting of 9 electrons in 12 orbitals, see Figure 4. But in contrast to the sextet case, the number of spin-adapted CSFs is 47240 and therefore about half as large as the number of ONVs. It should be emphasized that the number of variational parameters for the CGTNS ansatz here is the same as in the case

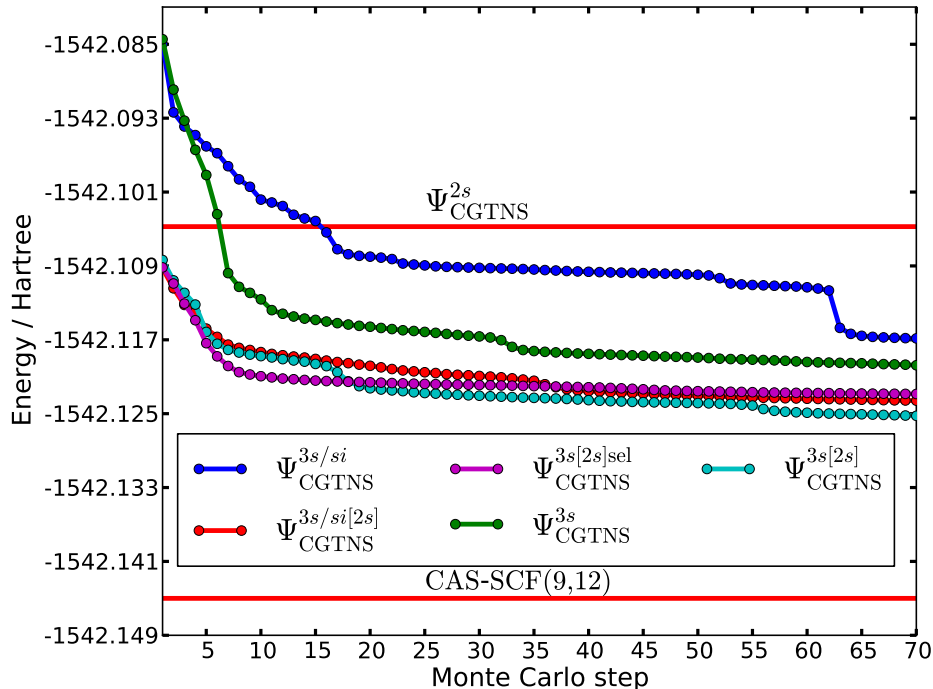
of the sextet, as it depends only on the number of spin orbitals in the active space. The 2-site correlator CGTNS scheme reduces the number of variational parameters by 99% with an error of about 40 mHartree, see Table III. Ψ_{CGTNS}^{3s} introduces 20800 variational parameters, which corresponds to a 80% reduction. For $\Psi_{\text{CGTNS}}^{3s/si}$ the reduction is larger (85%), corresponding to 16192 variational parameters.

Table III: Electronic energies for the doublet state of mangano-cene calculated with various CGTNS parameterizations and CAS-SCF(9,12). A percentage indicates a decreased parameter space compared to the 98060 CI coefficients in the CAS-SCF(9,12) reference calculation.

parameterization	parameters	percentage	energy/Hartree
CAS-SCF(9,12)	98060		-1542.144937
Ψ_{CGTNS}^{2s}	1200	99%	-1542.104681
$\Psi_{\text{CGTNS}}^{3s/si}$	16192	85%	-1542.116784
Ψ_{CGTNS}^{3s}	20800	80%	-1542.119695
$\Psi_{\text{CGTNS}}^{3s/si[2s]}$	16192	85%	-1542.123527
$\Psi_{\text{CGTNS}}^{3s[2s]}$	20800	80%	-1542.125171
$\Psi_{\text{CGTNS}}^{3s[2s]\text{sel}}$	9120	91%	-1542.122804
$\Psi_{\text{CGTNS}}^{3s+[2s]\text{sel}}$	9120	91%	-1542.123885

The $\Psi_{\text{CGTNS}}^{3s/si}$ and Ψ_{CGTNS}^{3s} parameterizations decrease the energy by -0.012103 and -0.015014 Hartree, respectively, see Table III. From Figure 8, it is obvious that 3-site correlators are important for energy minimization. As in the case of the sextet state, convergence is accelerated with information obtained from the 2-site correlators. As expected, incorporating 3-site correlators into the 2-site correlator ansatz ($\Psi_{\text{CGTNS}}^{3s/si[2s]}$ and $\Psi_{\text{CGTNS}}^{3s[2s]}$) yields energies close (and lower) to the one of the 2-site correlator ansatz right from the start, see Figure 8. In contrast to the sextet state, both hybrid parameterizations, $\Psi_{\text{CGTNS}}^{3s/si[2s]}$ and $\Psi_{\text{CGTNS}}^{3s[2s]}$, minimize the doublet energies further than the pure 3-site correlator schemes, yielding -1542.123527 and -1542.125171 Hartree, respectively.

Figure 8: Convergence behavior of 3-site correlator CGTNS parameterizations for manganocene in the doublet state.

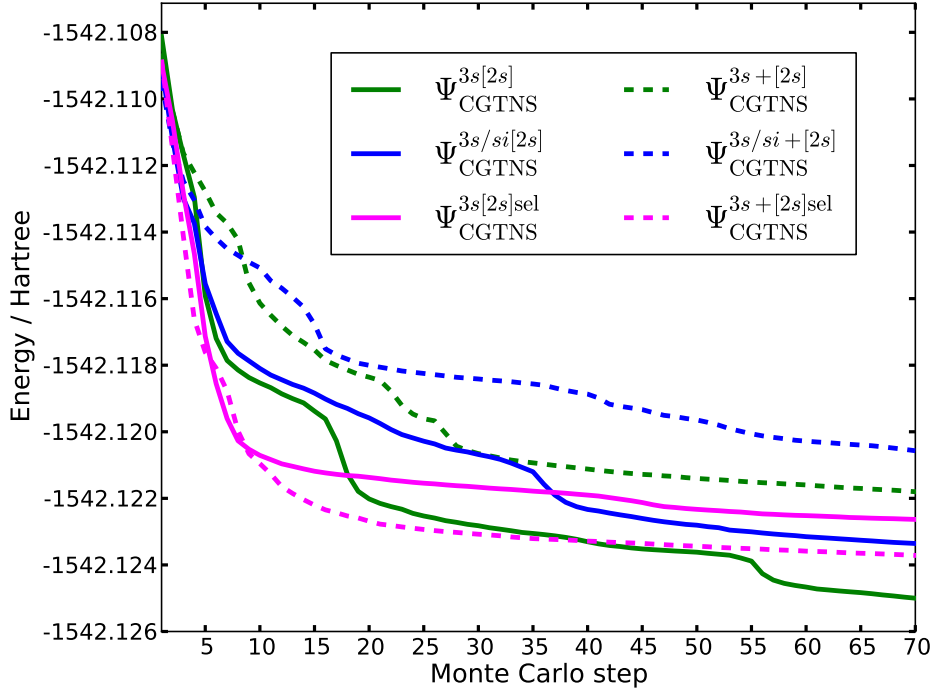


As for the sextet, we study whether all of the 3-site correlators are equally important in the wave function parameterization. Again, we choose the 18 most entangled spin orbitals according to the selection criterion in Section 3, resulting from natural orbitals **D-1, D-2, D-4, D-5, D-6, D-9, D-10, D-11, D-12**, see Figure 4. The corresponding hybrid CGTNS ansatz, $\Psi_{\text{CGTNS}}^{3s[2s]\text{sel}}$, has only 9120 variational parameters compared to 20800 in the $\Psi_{\text{CGTNS}}^{3s[2s]}$ ansatz. We observe that the chosen 3-site correlators are important for energy minimization. One can clearly see in Figure 8 that $\Psi_{\text{CGTNS}}^{3s[2s]\text{sel}}$ shows even faster convergence and the final energy is close to those of $\Psi_{\text{CGTNS}}^{3s/si[2s]}$ and $\Psi_{\text{CGTNS}}^{3s[2s]}$. Hence, the concept to include higher-order correlators in the CGTNS ansatz only for the most entangled orbitals is efficient.

In contrast to the sextet case, the hybrid schemes that employ a sum of 2-site and 3-site correlator products, $\Psi_{\text{CGTNS}}^{3s+[2s]}$ and $\Psi_{\text{CGTNS}}^{3s/si+[2s]}$, show slower energy convergence than their analogs employing products between 2-site and 3-site correlators, $\Psi_{\text{CGTNS}}^{3s[2s]}$ and $\Psi_{\text{CGTNS}}^{3s/si[2s]}$, see Figure 9. The final energies obtained from $\Psi_{\text{CGTNS}}^{3s+[2s]}$ and $\Psi_{\text{CGTNS}}^{3s/si+[2s]}$ are higher than the ones obtained from their counterparts. An interesting behavior is exhibited by the $\Psi_{\text{CGTNS}}^{3s+[2s]\text{sel}}$ ansatz, see Figure 9. Although at the beginning, it shows convergence similar

to that of the $\Psi_{\text{CGTNS}}^{3s[2s]\text{sel}}$ ansatz, at the point where the energy from the $\Psi_{\text{CGTNS}}^{3s[2s]\text{sel}}$ ansatz is almost converged, the $\Psi_{\text{CGTNS}}^{3s+[2s]\text{sel}}$ ansatz succeeded to overcome local minima and the energy decreases further by 1.081 mHartree, see Table III and Figure 9.

Figure 9: Convergence behavior of hybrid CGTNS parameterizations for manganocene in the doublet state.



4.4 Accuracy Measure

So far, we observed two peculiarities of the CGTNS ansatz. In the case of the sextet state, the 2-site correlator parameterization provides an accurate approximation to the reference wave function and the introduction of higher-order correlators hardly changes the energy any further, in the best case by only -0.003705 Hartree. By contrast, Ψ_{CGTNS}^{2s} does not provide an adequate energy estimate for the doublet state of manganocene and 3-site correlators are needed to decrease the energy by -0.02049 Hartree. In the light of these observations, it is necessary to introduce a measure for the accuracy of CGTNS parameterizations and for the decision whether higher-order correlators should be introduced or not. For example, the small energy difference of $\Psi_{\text{CGTNS}}^{3s[2s]}$ compared to its extension to 3-site correlators in the $\Psi_{\text{CGTNS}}^{3s[2s]}$ ansatz,

$$\Delta E_{\text{CGTNS}}^{2s/3s} = E_{\text{CGTNS}}^{3s[2s]} - E_{\text{CGTNS}}^{2s}, \quad (33)$$

clearly shows that the introduction of 3-site correlators will not improve the energy. Such an energy-difference measure can serve for accuracy control. In the general case of n -site correlators, it is given by

$$\Delta E_{\text{CGTNS}}^{n/(n+1)s} = E_{\text{CGTNS}}^{(n+1)s[ns]} - E_{\text{CGTNS}}^{ns}. \quad (34)$$

As the next tier of approximation, $\Psi_{\text{CGTNS}}^{(n+1)s[ns]}$, may dramatically inflate the variational space, we insert the approximation $\Psi_{\text{CGTNS}}^{(n+1)s[ns]\text{sel}}$ instead of $\Psi_{\text{CGTNS}}^{(n+1)s[ns]}$,

$$\Delta E_{\text{CGTNS}}^{n/(n+1)s} \approx E_{\text{CGTNS}}^{(n+1)s[ns]\text{sel}} - E_{\text{CGTNS}}^{ns}. \quad (35)$$

The smaller variational space of a $\Psi_{\text{CGTNS}}^{(n+1)s[ns]\text{sel}}$ parameterization makes optimizations feasible and the energy usually converges within comparatively few Monte Carlo steps.

4.5 Manganocene — Spin-State Splitting

From Sections 4.2 and 4.3 it is obvious that energies obtained from low-order CGTNS parameterizations still deviate from the CAS-SCF reference. This may only be tolerated if relative energies are obtained with higher accuracy. We investigate this issue now for the spin-state splitting in manganocene. As we neglect dynamical correlation, our reference splitting is -40.59 kcal/mol (Table I). Since DFT results scatter by about 30 kcal/mol (Table I, see also⁵¹), we may consider a deviation by up to about 5 kcal/mol (10% of the CAS-SCF reference result) acceptable. If the simple strategy to use the same parameterization for both spin states is followed, two issues arise. The first one can be clearly seen if one takes the Ψ_{CGTNS}^{2s} ansatz for both spin states. For the sextet state, an accurate total energy is obtained, whereas for the doublet state the reduction of the variational space by 99% is so large that it leads to an inaccurate total energy. The energy difference then mounts to -56.09 kcal/mol, see Table IV. The problem here is that the configurational space for the doublet is 10 times larger than the one for the sextet, while the number of CGTNS variational parameters is equal. The second issue can be observed for the $\Psi_{\text{CGTNS}}^{3s[2s]}$ parameterization applied for both spin states. Then, the energy difference is equal to -44.00 kcal/mol, whereas the variational space for the sextet was enlarged by 59% relative to the CAS-SCF configurational space. Using the same ansatz for both states therefore introduces an imbalance in the approximation of the two different configurational spaces.

A reasonable strategy is to choose those parameterizations which reduce the variational space by the same amount and are therefore likely to be affected by similar errors. For manganocene, $\Psi_{\text{CGTNS}}^{3s[2s]\text{sel}}$ achieves a reduction by 91% of the variational space for the

doublet state, while for the sextet state the same reduction is achieved by the Ψ_{CGTNS}^{2s} ansatz. The energy difference estimated based on these schemes is -44.72 kcal/mol. If the $\Psi_{\text{CGTNS}}^{3s+[2s]\text{sel}}$ scheme is used instead, the energy difference is equal to -44.04 kcal/mol.

Table IV: The doublet–sextet energy differences in Hartree and kcal/mol for manganocene calculated with various CGTNS parameterizations and CAS-SCF(9,12).

parameterization		$E[{}^6A_1] - E[{}^2A_1]$	
6A_1	2A_1	Hartree	kcal/mol
CAS-SCF(9,12)	CAS-SCF(9,12)	-0.064683	-40.59
Ψ_{CGTNS}^{2s}	Ψ_{CGTNS}^{2s}	-0.089391	-56.09
$\Psi_{\text{CGTNS}}^{3s/si[2s]}$	$\Psi_{\text{CGTNS}}^{3s/si[2s]}$	-0.071888	-45.11
$\Psi_{\text{CGTNS}}^{3s[2s]}$	$\Psi_{\text{CGTNS}}^{3s[2s]}$	-0.070112	-44.00
$\Psi_{\text{CGTNS}}^{3s/si}$	$\Psi_{\text{CGTNS}}^{3s/si}$	-0.078955	-49.55
Ψ_{CGTNS}^{3s}	Ψ_{CGTNS}^{3s}	-0.078082	-49.00
$\Psi_{\text{CGTNS}}^{3s[2s]\text{sel}}$	$\Psi_{\text{CGTNS}}^{3s[2s]\text{sel}}$	-0.072022	-45.20
$\Psi_{\text{CGTNS}}^{3s+[2s]\text{sel}}$	$\Psi_{\text{CGTNS}}^{3s+[2s]\text{sel}}$	-0.070936	-44.51
Ψ_{CGTNS}^{2s}	$\Psi_{\text{CGTNS}}^{3s[2s]\text{sel}}$	-0.071269	-44.72
Ψ_{CGTNS}^{2s}	$\Psi_{\text{CGTNS}}^{3s+[2s]\text{sel}}$	-0.070187	-44.04

The energy differences calculated with other 3-site correlator schemes are presented in Table IV. The $\Psi_{\text{CGTNS}}^{3s/si[2s]}$ ansatz performs slightly worse than the $\Psi_{\text{CGTNS}}^{3s[2s]}$ ansatz for the spin-state splitting energy giving -45.11 kcal/mol. Approximately the same result, -45.20 kcal/mol, can be obtained if the $\Psi_{\text{CGTNS}}^{3s[2s]\text{sel}}$ ansatz is employed in both spin-state calculations. The energy difference obtained from the $\Psi_{\text{CGTNS}}^{3s+[2s]\text{sel}}$ ansatz is equal to -44.51 kcal/mol. Whereas in the case of the 3-site CGTNS schemes employing correlators for all spin orbitals the variational space for the sextet state is enlarged compared to the CAS-CI space in a reference calculation, the $\Psi_{\text{CGTNS}}^{3s[2s]\text{sel}}$ and $\Psi_{\text{CGTNS}}^{3s+[2s]\text{sel}}$ ansätze reduce the variational space not only for the doublet state but also for the sextet state (66%). The results obtained from $\Psi_{\text{CGTNS}}^{3s/si}$ and Ψ_{CGTNS}^{3s} parameterizations are nearly the same and equal to -49.55 kcal/mol and -49.00 kcal/mol, respectively. Note that these schemes enlarge the variational space for the sextet to the same extent as their hybrid analogs.

5 Conclusions

In this paper, we presented a rigorous analysis of various n -site correlators schemes for tensor network states at the example of manganocene. We demonstrated that the 2-

site correlator CGTNS scheme achieves an efficient parameter reduction for the systems with a configurational space spanned by about 15 000 ONVs. In the case of the sextet state of manganocene, the number of variational parameters is reduced by 91% without significant loss of accuracy; the error is about 15.5 mHartree.

Introducing higher-order correlators increases the accuracy and delivers results closer to the CAS-SCF reference results. This, however, comes with an unreasonable inflation of the parameter space. We suggested and analyzed two different strategies for the introduction of higher-order correlators. The first one assumes that the ansatz features only 3-site correlators and optimizes the energy with respect to them alone. The second strategy incorporates 3-site correlators into a converged 2-site correlator ansatz. We demonstrated that such a hybrid extension of a 2-site correlator ansatz converges better and faster than the optimization of only 3-site correlators. The 3-site correlator CGTNS parameterizations are accurate for the description of a configurational space of about 100 000 ONVs. One can avoid inflation of the variational space by considering 3-site correlators only for the most entangled spin orbitals. Such a restriction has only a slight affect on accuracy with respect to the original ansatz; in addition, it also increases energy convergence in the Monte Carlo optimization.

Our results for the doublet state of manganocene showed that a reduction of the variational space by 80%, 85%, 91%, and 99% leads to errors of only -19.766 mHartree, -21.41 mHartree, 23.174 mHartree, and -40.256 mHartree, respectively. Therefore, only an adaptive CGTNS ansatz is promising that introduces higher-order correlators selectively on demand. With the energy measures introduced for accuracy control such an ansatz can adapt to the electronic structure under the study.

A reduction of variational space by 85% to 90% leads to a 20 mHartree error for total electronic energies. However, for most chemical processes, the evaluation of energy *differences* is most important. We found that reliable results can be obtained if the same reduction of variational parameters for the two energies to be compared is achieved. For the manganocene sextet–doublet energy difference, the error introduced by tensor network parameterizations can be reduced to only 8.5% of the reference value.

While the non-stochastic optimization schemes performed well for the CPS ansatz, for CGTNS they turned out to be inefficient. Hence, additional work on the improvement of our Monte Carlo optimization scheme is required. A possibility is the introduction of dynamically optimized temperature sets.⁷⁶

6 Acknowledgment

This work was supported by ETH Zurich (ETH Fellowship FEL-27 14-1).

References

- [1] S. WHITE, *Phys. Rev. Lett.* **69**, 2863 (1992).
- [2] U. SCHOLLWÖCK, *Rev. Mod. Phys.* **77**, 259 (2005).
- [3] U. SCHOLLWÖCK, *Ann. Phys.* **326**, 96 (2011).
- [4] Ö. LEGEZA, R. NOACK, J. SÓLYOM, and L. TINCANI, *Lect. Notes Phys.* **739**, 653 (2008).
- [5] G. K.-L. CHAN, J. J. DORANDO, D. GHOSH, J. HACHMANN, E. NEUSCAMMAN, H. WANG, and T. YANAI, *Prog. Theor. Chem. Phys.* **18**, 49 (2008).
- [6] G. K.-L. CHAN and D. ZGID, *Annu. Rep. Comput. Chem.* **5**, 149 (2009).
- [7] K. H. MARTI and M. REIHER, *Z. Phys. Chem.* **224**, 583 (2010).
- [8] G. K.-L. CHAN and S. SHARMA, *Ann. Rev. Phys. Chem.* **62**, 465 (2011).
- [9] K. H. MARTI and M. REIHER, *Phys. Chem. Chem. Phys.* **13**, 6750 (2011).
- [10] S. F. KELLER and M. REIHER, *Chimia* **68**, 200 (2014).
- [11] Y. KURASHIGE, *Mol. Phys.* **112**, 1485 (2014).
- [12] WOUTERS, SEBASTIAN and VAN NECK, DIMITRI, *Eur. Phys. J. D* **68**, 272 (2014).
- [13] T. YANAI, Y. KURASHIGE, W. MIZUKAMI, J. CHALUPSKÝ, T. N. LAN, and M. SAITOW, *Int. J. Quantum Chem.* **115**, 283 (2015).
- [14] S. SZALAY, M. PFEFFER, V. MURG, G. BARCZA, F. VERSTRAETE, R. SCHNEIDER, and Ö. LEGEZA, *Int. J. Quantum Chem.* **115**, 1342 (2015).
- [15] S. KNECHT, E. D. HEDEGÅRD, S. KELLER, A. KOVYRHSIN, Y. MA, A. MUOLO, C. J. STEIN, and M. REIHER, *Chimia* **70**, 244 (2016).

- [16] F. AQUILANTE, J. AUTSCHBACH, R. K. CARLSON, L. F. CHIBOTARU, M. G. DELCEY, L. DE VICO, I. FDEZ. GALVÁN, N. FERRÉ, L. M. FRUTOS, L. GAGLIARDI, M. GARAVELLI, A. GIUSSANI, C. E. HOYER, G. LI MANNI, H. LISCHKA, D. MA, P. Å. MALMQVIST, T. MÜLLER, A. NENOV, M. OLIVUCCI, T. B. PEDERSEN, D. PENG, F. PLASSER, B. PRITCHARD, M. REIHER, I. RIVALTA, I. SCHAPIRO, J. SEGARRA-MARTÍ, M. STENRUP, D. G. TRUHLAR, L. UNGUR, A. VALENTINI, S. VANCOILLIE, V. VERYAZOV, V. P. VYSOTSKIY, O. WEINGART, F. ZAPATA, and R. LINDH, *J. Comput. Chem.* **37**, 506 (2016).
- [17] S. ÖSTLUND and S. ROMMER, *Phys. Rev. Lett.* **75**, 3537 (1995).
- [18] K. H. MARTI, I. MALKIN ONDIK, G. MORITZ, and M. REIHER, *J. Chem. Phys.* **128**, 014104 (2008).
- [19] Y. KURASHIGE and T. YANAI, *J. Chem. Phys.* **135**, 094104 (2011).
- [20] S. SHARMA and G. K.-L. CHAN, *J. Chem. Phys.* **141**, 111101 (2014).
- [21] S. GUO, M. WATSON, W. HU, Q. SUN, and G. K.-L. CHAN, *J. Chem. Theor. Comput.* **12**, 1583 (2016).
- [22] E. FROMAGER, J. TOULOUSE, and H. J. Å. JENSEN, *J. Chem. Phys.* **126**, 074111 (2007).
- [23] E. D. HEDEGÅRD, S. KNECHT, J. S. KIELBERG, H. J. A. JENSEN, and M. REIHER, *J. Chem. Phys.* **142**, 224108 (2015).
- [24] T. NISHINO, K. OKUNISHI, Y. HIEIDA, N. MAESHIMA, and Y. AKUTSU, *Nucl. Phys. B* **575**, 504 (2000).
- [25] T. NISHINO, Y. HIEIDA, K. OKUNISHI, N. MAESHIMA, Y. AKUTSU, and A. GENDIAR, *Prog. Theor. Phys.* **105**, 409 (2001).
- [26] A. GENDIAR and T. NISHINO, *Phys. Rev. E* **65**, 046702 (2002).
- [27] A. GENDIAR, N. MAESHIMA, and T. NISHINO, *Prog. Theor. Phys.* **110**, 691 (2003).
- [28] N. SCHUCH, M. M. WOLF, F. VERSTRAETE, and J. I. CIRAC, *Phys. Rev. Lett.* **100**, 040501 (2008).
- [29] F. VERSTRAETE and J. I. CIRAC, *arXiv:cond-mat/0407066* (2004).

- [30] G. EVENBLY and G. VIDAL, *Phys. Rev. Lett.* **112**, 240502 (2014).
- [31] F. MEZZACAPO, N. SCHUCH, M. BONINSEGNI, and J. I. CIRAC, *New J. Phys.* **11**, 083026 (2009).
- [32] H. CHANGLANI, J. KINDER, C. UMRIGAR, and G. KIN-LIC CHAN, *Phys. Rev. B* **80**, 245116 (2009).
- [33] K. MARTI, B. BAUER, M. REIHER, M. TROYER, and F. VERSTRAETE, *New J. Phys.* **12**, 103008 (2010).
- [34] V. MURG, F. VERSTRAETE, O. LEGEZA, and R. M. NOACK, *Phys. Rev. B* **82**, 205105 (2010).
- [35] G. BARCZA, O. LEGEZA, K. H. MARTI, and M. REIHER, *Phys. Rev. A* **83**, 012508 (2011).
- [36] N. NAKATANI and G. K.-L. CHAN, *J. Chem. Phys.* **138**, 134113 (2013).
- [37] E. NEUSCAMMAN, C. UMRIGAR, and G. K. CHAN, *Phys. Rev. B* **85**, 045103 (2012).
- [38] E. NEUSCAMMAN and G. K. CHAN, *Phys. Rev. B* **86**, 064402 (2012).
- [39] P. JOHNSON, P. AYERS, P. LIMACHER, S. DE BAERDEMACKER, D. VAN NECK, and P. BULTINCK, *Comp. Theor. Chem.* **1003**, 101 (2013).
- [40] P. LIMACHER, P. AYERS, P. JOHNSON, S. DE BAERDEMACKER, D. VAN NECK, and P. BULTINCK, *J. Chem. Theory Comput.* **9**, 1394 (2013).
- [41] O. LEGEZA and J. SÓLYOM, *Phys. Rev. B* **68**, 195116 (2003).
- [42] O. LEGEZA and J. SÓLYOM, *Phys. Rev. B* **70**, 205118 (2004).
- [43] J. RISSLER, R. M. NOACK, and S. R. WHITE, *Chem. Phys.* **323**, 519 (2006).
- [44] K. BOGUSLAWSKI, P. TECMER, O. LEGEZA, and M. REIHER, *J. Phys. Chem. Lett.* **3**, 3129 (2012).
- [45] C. J. STEIN and M. REIHER, *J. Chem. Theor. Comput.* **12**, 1760 (2016).
- [46] A. SANDVIK and G. VIDAL, *Phys. Rev. Lett.* **99**, 220602 (2007).
- [47] G. BOOTH, A. THOM, and A. ALAVI, *J. Chem. Phys.* **131**, 054106 (2009).
- [48] J. SHEPHERD, G. BOOTH, and A. ALAVI, *J. Chem. Phys.* **136**, 244101 (2012).

- [49] G. BOOTH, A. GRUNEIS, G. KRESSE, and A. ALAVI, *Nature* **493**, 365 (2013).
- [50] W. PRESS, S. TEUKOLSKY, W. VETTERLING, and B. FLANNERY, *Numerical Recipes 3rd Edition: The Art of Scientific Computing*, Cambridge University Press, New York, NY, USA, 3 edition, 2007.
- [51] O. SALOMON, M. REIHER, and B. HESS, *J. Chem. Phys.* **117**, 4729 (2002).
- [52] Q. M. PHUNG, S. VANCOILLIE, and K. PIERLOOT, *J. Chem. Theory Comput.* **8**, 883 (2012).
- [53] C. J. STEIN, V. VON BURG, and M. REIHER, *arXiv*, online (2016).
- [54] E. FROMAGER, J. TOULOUSE, and H. J. A. JENSEN, *J. Chem. Phys.* **126**, 074111 (2007).
- [55] TURBOMOLE V6.5 2013, a development of University of Karlsruhe and Forschungszentrum Karlsruhe GmbH, 1989-2007, TURBOMOLE GmbH; available from <http://www.turbomole.com>.
- [56] R. AHLRICH, M. BÄR, M. HÄSER, H. HORN, and C. KÖLMEL, *Chem. Phys. Lett.* **162**, 165 (1989).
- [57] J. P. PERDEW, M. ERNZERHOF, and K. BURKE, *J. Chem. Phys.* **105**, 9982 (1996).
- [58] F. WEIGEND, M. HÄSER, H. PATZELT, and R. AHLRICH, *Chem. Phys. Lett.* **294**, 143 (1998).
- [59] F. WEIGEND, F. FURCHE, and R. AHLRICH, *J. Chem. Phys.* **119**, 12753 (2003).
- [60] J. P. PERDEW, K. BURKE, and M. ERNZERHOF, *Phys. Rev. Lett.* **77**, 3865 (1996).
- [61] S. GRIMME, J. ANTONY, S. EHRLICH, and H. KRIEG, *J. Chem. Phys.* **132**, 154104 (2010).
- [62] B. A. HESS, *Phys. Rev. A* **33**, 3742 (1986).
- [63] A. WOLF, M. REIHER, and B. A. HESS, *J. Chem. Phys.* **117**, 9215 (2002).
- [64] M. REIHER and A. WOLF, *J. Chem. Phys.* **121**, 2037 (2004).
- [65] D. PENG, N. MIDDENDORF, F. WEIGEND, and M. REIHER, *J. Chem. Phys.* **138**, 184105 (2013).

- [66] P. WIDMARK, P. MALMQVIST, and B. ROOS, *Theor. Chim. Acta* **77**, 291 (1990).
- [67] B. ROOS, R. LINDH, P. MALMQVIST, V. VERYAZOV, and P. WIDMARK, *J. Phys. Chem. A* **108**, 2851 (2004).
- [68] B. ROOS, R. LINDH, P. MALMQVIST, V. VERYAZOV, and P. WIDMARK, *J. Phys. Chem. A* **109**, 6575 (2005).
- [69] F. AQUILANTE and R. L. T. B. PEDERSEN, *J. Chem. Phys.* **127**, 114107 (2007).
- [70] D. PENG and M. REIHER, *Theor. Chem. Acc.* **131**, 1081 (2012).
- [71] P. PULAY and T. HAMILTON, *J. Chem. Phys.* **88**, 4926 (1988).
- [72] J. BOFILL and P. PULAY, *J. Chem. Phys.* **90**, 3637 (1989).
- [73] S. KELLER, K. BOGUSLAWSKI, T. JANOWSKI, M. REIHER, and P. PULAY, *J. Chem. Phys.* **142**, 244104 (2015).
- [74] K. ANDERSSON, P. MALMQVIST, and B. O. ROOS, *J. Chem. Phys.* **96**, 1218 (1992).
- [75] C. ANGELI, R. CIMIRAGLIA, S. EVANGELISTI, T. LEININGER, and J.-P. MALRIEU, *J. Chem. Phys.* **114**, 10252 (2001).
- [76] H. G. KATZGRABER, S. TREBST, D. A. HUSE, and M. TROYER, *J. Stat. Mech. Theor. Exp.* **2006**, P03018 (2006).